# Dimethylcethrene: A Chiroptical Diradicaloid Photoswitch

Prince Ravat,[†,‡] Tomáš Šolomek,[†] Daniel Häussinger,[†] Olivier Blacque,[§] and Michal Juríček*[,†,§]

[†]Department of Chemistry, University of Basel, St. Johanns-Ring 19, CH-4056 Basel, Switzerland

[‡]Department of Chemistry, The University of Tokyo, 7-3-1 Hongo, Bunkyo-ku, Tokyo 113-0033, Japan

[§]Department of Chemistry, University of Zurich, Winterthurerstrasse 190, CH-8057 Zurich, Switzerland

# MAIN TEXT

## TABLE OF CONTENTS

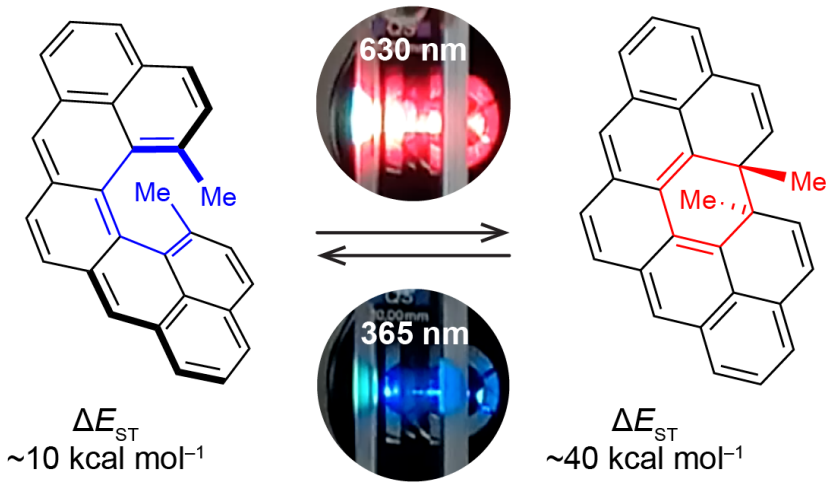


**ABSTRACT:** We describe the synthesis and properties of 13,14-dimethylcethrene, a prototype of a chiral diradicaloid photochemical switch that can be transformed reversibly via conrotatory electrocyclization to its more stable closed form by light (630 nm) or heat and back to its open form by light (365 nm). This system illustrates how chemical reactivity of a diradicaloid molecule can be translated into a switching function, which alters substantially all electronic parameters, namely, the HOMO–LUMO and the singlet–triplet (ST) energy gaps, and the degree of helical twist. As a result, distinct changes in the optical and chiroptical properties of this system were observed, which allowed us to monitor the switching process by a variety of spectroscopic techniques, including NMR, UV–vis, and CD. Compared to the previously reported parent molecule cethrene, this system benefits from two methyl substituents installed in the fjord region, which account for the stability of the closed form against oxidation and racemization. The methyl substituents increase the ST energy gap of 13,14-dimethylcethrene by ~4 kcal $mol^{-1}$ compared to cethrene. Our DFT calculations reveal that the larger ST gap is a result of electronic and geometric effects of the methyl substituents and show the potential of this system to act as a magnetic switch.

## INTRODUCTION

Spin-delocalized π-conjugated molecules[1] that contain one or more unpaired electrons hold promise as components of materials, which exhibit[2] magnetic and conducting properties that are typically associated with metals. While magnetism in these systems arises from the presence[3] of unpaired electrons in the ground or low-lying excited states, conductivity emerges on account of the short (~3.1–3.2 Å) intermolecular distance[4] between the molecules that are held[5] together via multi-centered *n*-electron π-bonds, also referred to as "pancake bonds". These bonds can be formed by favorable overlap of singly occupied molecular orbitals (SOMOs) in odd-electron[4] or non-Kekulé[6] systems, or by favorable overlap of partially occupied frontier molecular orbitals (FMOs; namely, HOMO and LUMO) in the so-called "diradicaloid" Kekulé[2b] systems. In the latter case, the non-degenerate FMOs are close in energy and, as a consequence, a pair of electrons from the HOMO (*a*) partially occupies also the LUMO (*b*) to minimize electron repulsion. The singlet ground state of these molecules is therefore best described[7] by mixing a doubly excited configuration $a^0b^2$ into the ground-state configuration $a^2b^0$. In addition to the low-lying LUMO, a common feature of diradicaloid molecules is the presence[3] of a low-lying triplet excited state, which can be populated[1] thermally.

In the pursuit of identifying structural features that would allow for fine-tuning of key electronic parameters of diradicaloids, namely, the HOMO–LUMO and ST gaps, we turned our attention to systems that feature a helical π-conjugated backbone. On account of the helical structure of these systems, through-space orbital interactions arise[8] within their FMOs, which can increase or decrease the FMO energies. Helical geometry is also the source of chirality[9] and can create favorable steric environment for certain intramolecular bond-rearrangement reactions, which, as we shall see, can be translated into a switching function. Recently, we developed[10] the first model system of this type, a C-shaped hydrocarbon

cethrene (o-**1**; Scheme 1, top), composed of seven fused benzenoid rings, five of which form a [5]helicene backbone. By synthesizing a diphenyl derivative o-**1a**, we were able to demonstrate[11] its several unique features: (1) The helical geometry gives rise to through-space orbital interactions at positions 13 and 14, namely, an antibonding within the HOMO and a bonding within the LUMO (see Figure 5a). These interactions decrease[11c] both (a) the HOMO–LUMO gap (1.68 eV, DFT) and (b) the ST gap (5.9 kcal $mol^{-1}$, DFT) of o-**1a**, when compared to a planar diradicaloid isomer heptazethrene[12] (HOMO–LUMO gap of 1.79 eV, ST gap of 8.9 kcal $mol^{-1}$, DFT[11c]), rendering o-**1a** EPR active (ST gap of 5.6 kcal $mol^{-1}$, EPR). (2) Cethrene o-**1a** undergoes an electrocyclic ring-closure to a more stable closed form c-**1a** (Scheme 1, top), which proceeds in a conrotatory mode on account of steric constraints enforced by the helical geometry. Unlike most of other electrocyclic reactions, however, the conrotatory ring-closure of o-**1a** proceeds[11a] both (a) photochemically, which is a symmetry-allowed[13] reaction, as well as (b) thermally with a surprisingly low activation barrier (~14 kcal $mol^{-1}$), formally a symmetry-forbidden[13] reaction, the mechanism of which is not fully understood.

Because of a facile oxidation of c-**1a** to a planar hydrocarbon **2a**, which did not allow us to isolate or even detect[11a] this intermediate, we were unable to perform the reversed reaction, namely, photochemical ring-opening of c-**1a** to o-**1a**. Nonetheless, this process could be validated in an analogous system biphenalenylidene[14] (o-**3**; Scheme 1, bottom) by Kubo and co-workers, who demonstrated[14a] that the closed form c-**3** underwent an electrocyclic ring-opening to give o-**3** upon irradiation by UV light. In analogy to o-**1a**, the open form o-**3** also underwent a thermal ring-closing reaction, which proceeded with a barrier (~16 kcal $mol^{-1}$) close to that of o-**1a**. In this case, however, irradiation of o-**3** by visible light in the solid matrix did not afford c-**3**. Similarly to c-**1a**, c-**3** also undergoes a facile oxidation to a planar hydrocarbon **4**.

**Scheme 1. An Overview of Electrocyclic Ring-Closures of Cethrene (Top, Middle) and Biphenalenylidene (Bottom) and Electrocyclic Ring-Openings and Oxidations of Their Closed Forms**

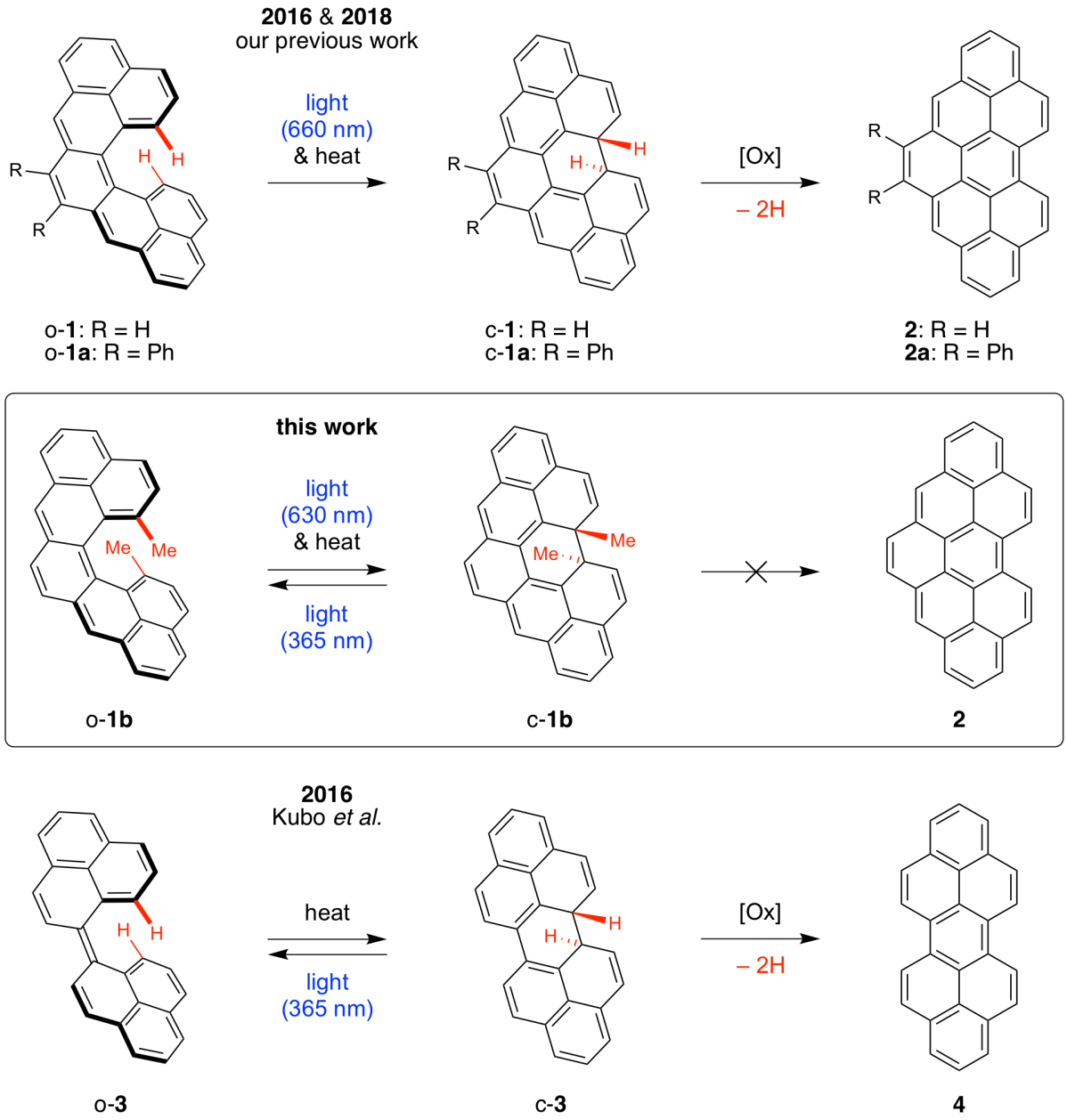


Our results and those of Kubo and co-workers indicate that chemical reactivity of cethrene and related diradicaloid molecules could be employed as a working principle in a switch that can be operated solely by light. In order to verify the reversibility of the photochemical ring-opening/-closing process and the ability of cethrene to act as a photoswitch, we designed and

herein present its derivative o-**1b** (Scheme 1, middle), equipped with two methyl substituents (in red) in place of two hydrogen atoms in the fjord region, which are critical for suppressing the oxidation of the closed form to the flat hydrocarbon **2**. In addition to improving the stability of c-**1b**, the methyl substituents expedite[15] the synthesis of the [5]helicene core as well as increase[15] its configurational stability. Our present results demonstrate that 13,14-dimethylcethrene can be switched reversibly between an open (o-**1b**) and a closed (c-**1b**) form by light, and we introduce this system as a prototype of a chiral diradicaloid photoswitch. During the switching process, the (1) HOMO–LUMO and (2) ST gaps as well as (3) the degree of helical twist are altered simultaneously, leading to significant changes in the optical and chiroptical properties. Furthermore, our DFT calculations suggest that additional decrease of the ST gap of the open form, which could be achieved by suitable structural modification, can make this system act also as a magnetic switch.

## RESULTS

**Synthesis.** Starting from **5**,[15] diester intermediate **6** was prepared (Scheme 2) through a palladium-catalyzed Heck cross-coupling reaction with methyl acrylate followed by a reduction in a yield of 73% over the two steps. Diester **6** was subsequently transformed first into a diacid and then its bis(acyl chloride), which afforded the key intermediate **7** in a Friedel–Crafts acylation mediated by $AlCl_3$ in a 43% yield over the three steps. Compound **7** contains all seven six-membered rings of the cethrene core, and its structure was confirmed by 1D/2D NMR spectroscopy (Sections S7 and S8) as well as X-ray crystallographic analysis (Section S5, SI). Finally, a reduction of **7** followed by a dehydration provided the dihydro-precursor **8** (61% over two steps), which upon oxidation with *p*-chloranil afforded the target compound c-**1b** in 91% yield. In the final step, the oxidant *p*-chloranil first generates the open

form o-**1b**, which undergoes an in-situ thermal electrocyclic ring-closure to yield the closed form c-**1b** that can be isolated by column chromatography as a stable compound.

**Scheme 2. Synthesis of the Closed Form of 13,14-Dimethylcethrene**[a]

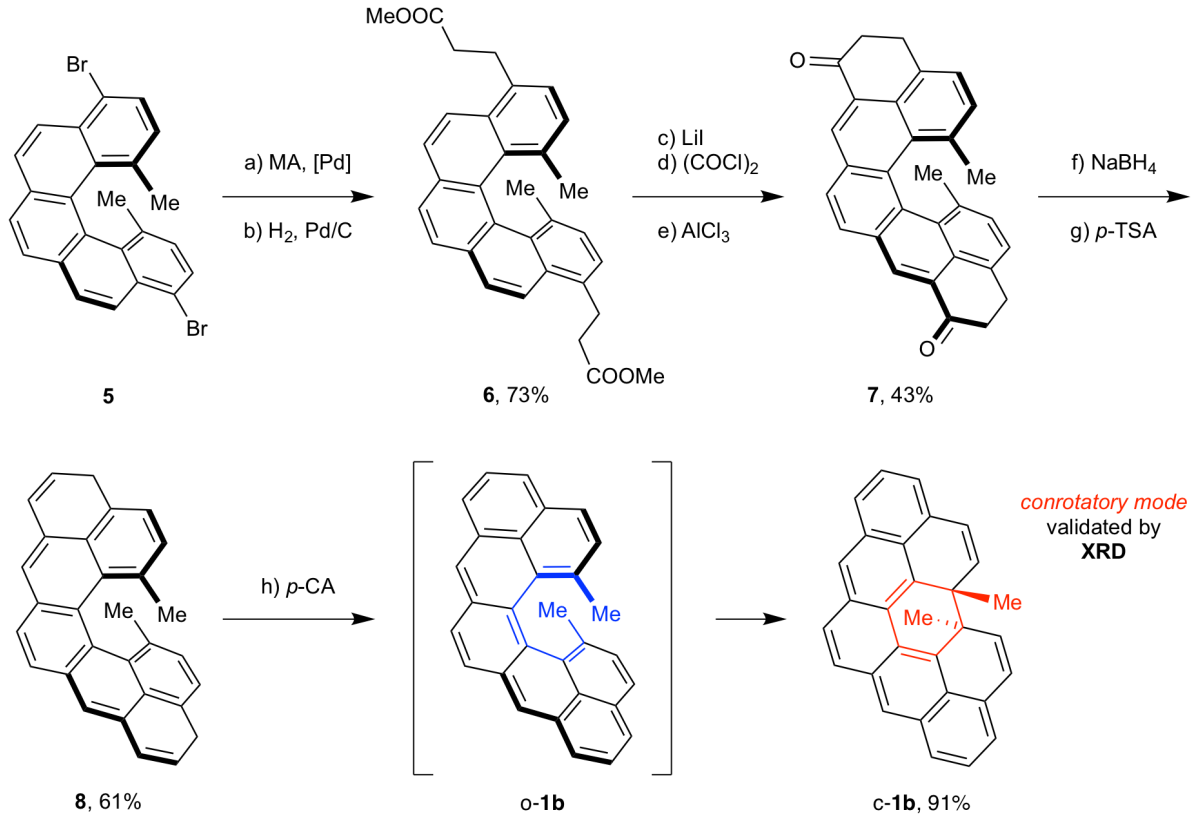


[a] Reaction conditions: (a) methyl acrylate (MA), $Pd(OAc)_2$, $PPh_3$, $K_2CO_3$, $Bu_4NBr$, DMF, 110 °C, 20 h; (b) $H_2$, Pd/C, $CH_2Cl_2$/EtOH, rt, 3 h; (c) LiI, 2,4,6-collidine, 185 °C, 3 h (d) $C_2O_2Cl_2$, 65 °C, 2.5 h; (e) $AlCl_3$, $CH_2Cl_2$, –78 to –10 °C, 5 h; (f) $NaBH_4$, $CH_2Cl_2$/EtOH, rt, 1.5 h; (g) *p*-TSA, toluene, 90 °C, 5 min; (h) *p*-chloranil, $C_6H_6$, rt, 16 h.

**Structural Characterization.** To validate the structures, the proton and carbon resonances for both c-**1b** and o-**1b** were fully assigned by a combination of COSY, NOESY, HMQC, and HMBC NMR techniques (Sections S7 and S8, SI). In the $^1$H NMR spectrum of c-**1b** (Figure 1, bottom), the resonances for protons H-1 and H-2 are in the region typical for a double bond

(6.2–6.7 ppm) in agreement with the crystal structure (vide infra; Figure 2). Resonances for protons H-3, H-4, H-5, H-6, and H-7 of the pentaphene moiety are in the aromatic region (6.9–7.8 ppm), the highest chemical shift being displayed by H-6 (~7.8 ppm).

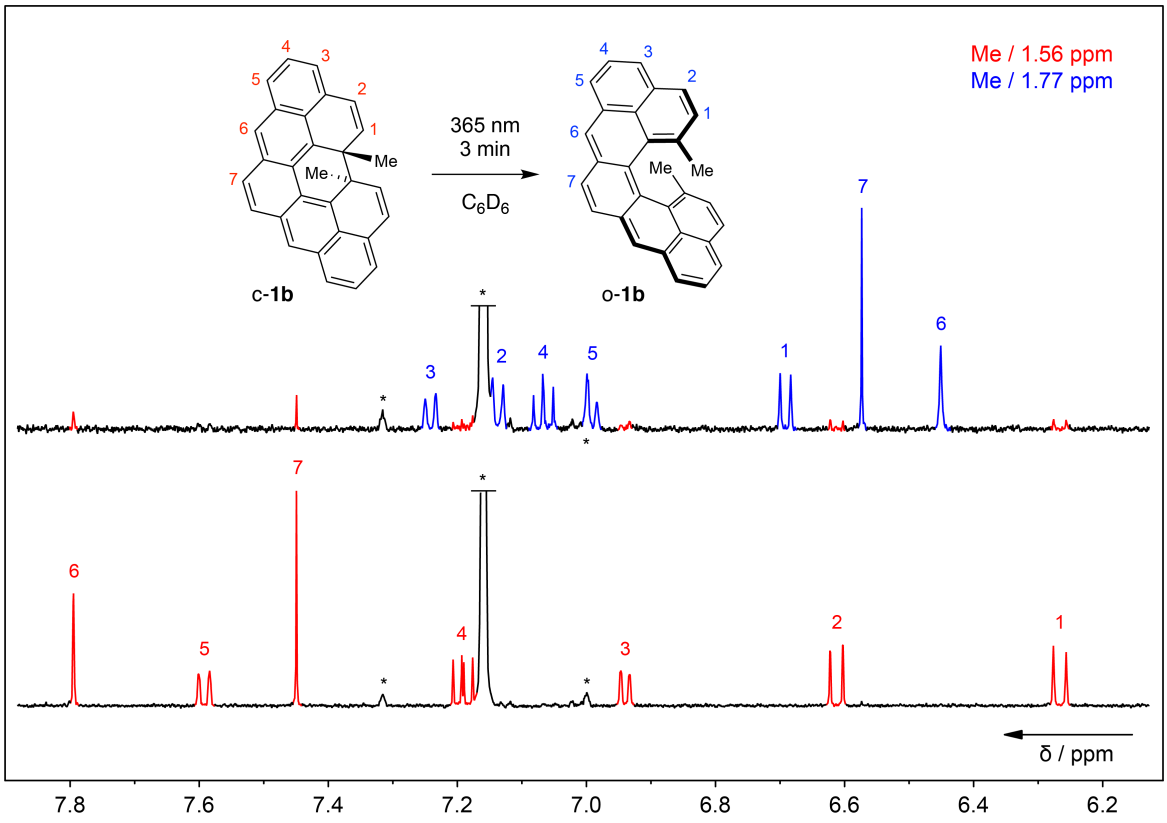


**Figure 1.** $^{1}$H NMR Spectra (600 MHz, $C_6D_6$, 25 °C) of c-**1b** (red) recorded before (bottom) and after (top) irradiation at 365 nm for 3 min, which generates o-**1b** (blue). The assignment of the proton resonances is shown (for 2D spectra, see the SI). Black asterisks denote the residual solvent and its satellite signals.

The structure of the open form o-**1b** was confirmed with a sample generated by irradiating a solution of c-**1b** (~$10^{-4}$ M in $C_6D_6$) at 365 nm for 3 min (Figure 1). Upon irradiation, the proton resonances of c-**1b** (in red) almost completely disappeared and the resonances that belong to o-**1b** (in blue) became visible (o-**1b**/c-**1b** ~ 7:1). In the $^{1}$H NMR spectrum of o-**1b**, the resonances for protons H-6 and H-7 are shifted upfield to 6.4–6.6 ppm, in accord with the

quinoidal structure (highlighted in blue in Figure 5b). The remaining proton resonances in the region 6.9–7.3 ppm reflect the aromatic character of the naphthalene subunits, except for the resonance of H-1 protons (6.68 ppm), which are shielded from the opposing terminal benzenoid ring.

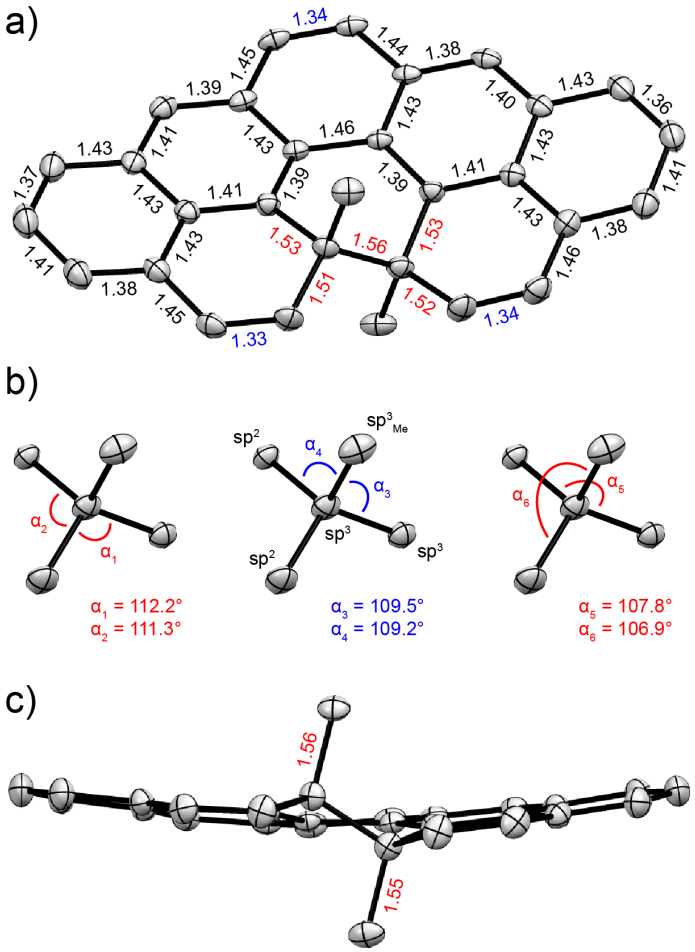


**Figure 2.** (a,c) The top (a) and side (c) views of the racemic solid-state structure of c-**1b** obtained from the single-crystal X-ray diffraction analysis. The thermal ellipsoids are shown at a 50% probability level and the bond lengths are given in Å. The bond-length values typical for single and double bonds are highlighted in red and blue, respectively. (b) Tetrahedral angles (α) of the $sp^3$-carbon atom bearing the methyl group. Angles with values close to an ideal tetrahedral angle value (~109.5°) are highlighted in blue and those that have higher (left) or lower (right) values are highlighted in red.

The structure of compound c-**1b** was also validated by X-ray crystallographic analysis (Figure 2 and Section S5, SI) of a single crystal grown from a hexane solution by slow evaporation of the solvent. The solid-state structure reveals an almost flat, slightly bent geometry of c-**1b**, with the two skeletal quaternary $sp^3$-carbon atoms each bearing one methyl substituent protruding above and below the skeleton plane. The structure appears to be only partially strained, judging from (1) slightly elongated $C(sp^3)$–$C(sp^3)$ (1.55–1.56 Å) and $C(sp^2)$–$C(sp^3)$ (1.51–1.53 Å) bonds (Figure 2a,c), (2) small bond-length alteration of the benzenoid rings (Figure 2a), and (3) minor distortion of some tetrahedral angles of the quaternary $sp^3$-carbon atoms from an ideal value of ~109.5° (Figure 2b).

**UV–Vis Kinetic Measurements.** The kinetic parameters of the thermal conrotatory electrocyclic ring-closure of o-**1b** to c-**1b**, namely, the rate constants ($k$) and the activation energy ($E_a$), were determined through UV–vis spectroscopic measurements in toluene and $CH_2Cl_2$. Compounds c-**1b** and o-**1b** have distinct UV–vis spectra (Figure 3a), where the former shows absorption mostly in the UV region (red trace), while the latter has a characteristic absorption band ($\lambda_{max}$ = 626 nm; $S_0$–$S_1$ transition) in the visible region (blue trace). In the kinetic studies, a solution of c-**1b** (~$10^{-4}$ M) was irradiated by light (365 nm), which provided o-**1b** via photochemical electrocyclic ring-opening reaction. Subsequently, the decrease of the absorbance ($A$) of o-**1b** at $\lambda_{max}$ = 626 nm in toluene and 624 nm in $CH_2Cl_2$ was followed in time ($t$) at various temperatures (Figures S1 and S2). The plot $\ln(A_t/A_0)$ against $t$ was used for determination of the $k$ values at specific temperatures ($T$) and then the plot $\ln(k)$ against $1/T$ was used to determine $E_a$ (Figures 3b, S3, and S4). In toluene, the ring-closure proceeds with an $E_a$ = (20.3 ± 0.26) kcal $mol^{-1}$, while $E_a$ = (17.1 ± 1.3) kcal $mol^{-1}$ in $CH_2Cl_2$.

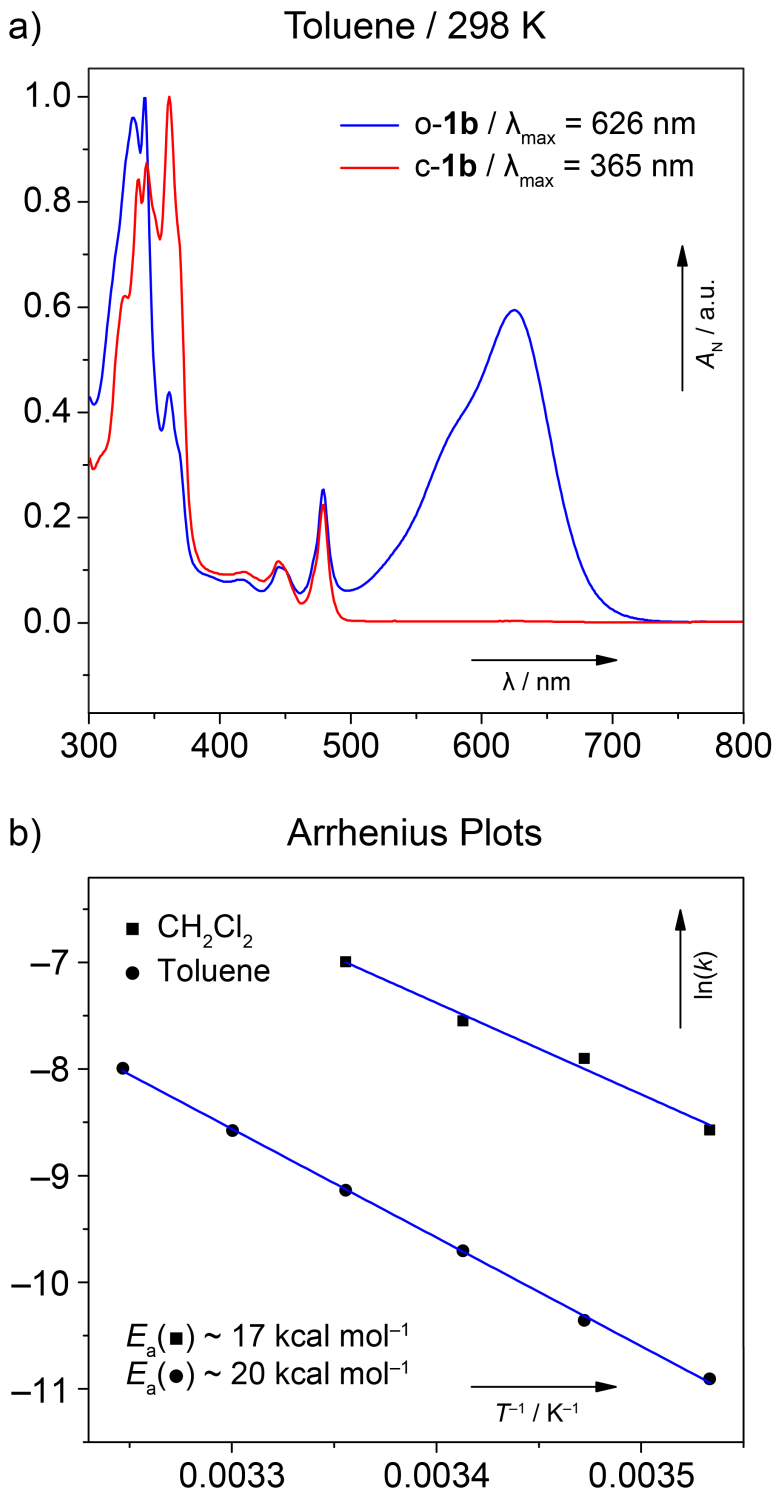


**Figure 3.** (a) Normalized UV–vis spectra of a solution of c-**1b** in toluene (~$10^{-4}$ M, 298 K) before (red trace) and after (blue trace) irradiation (365 nm, 1 min), which generates o-**1b**. The absorption bands of low intensity at 450 and 480 nm belong to an unknown impurity. (b) Arrhenius plots of ln($k$) against 1/$T$ used for determination of $E_a$ in $CH_2Cl_2$ and toluene.

**Circular Dichroism (CD) Spectroscopy.** The (*R*,*R*) and (*S*,*S*) enantiomers of c-**1b** were separated by HPLC employing a chiral stationary phase (Figure S8) and the absolute configuration of each enantiomer was assigned with the aid of TD-DFT calculations (Figure S9). The complementary CD spectra for both enantiomers are shown in Figure 4 (red traces). Irradiation (365 nm, 1 min) of the solution of (*R*,*R*)-c-**1b** generated the corresponding (*M*) enantiomer of o-**1b**, while the (*P*) enantiomer was obtained from (*S*,*S*)-c-**1b**. These enantiomers also displayed mirror-image Cotton effects in their CD spectra (blue traces).

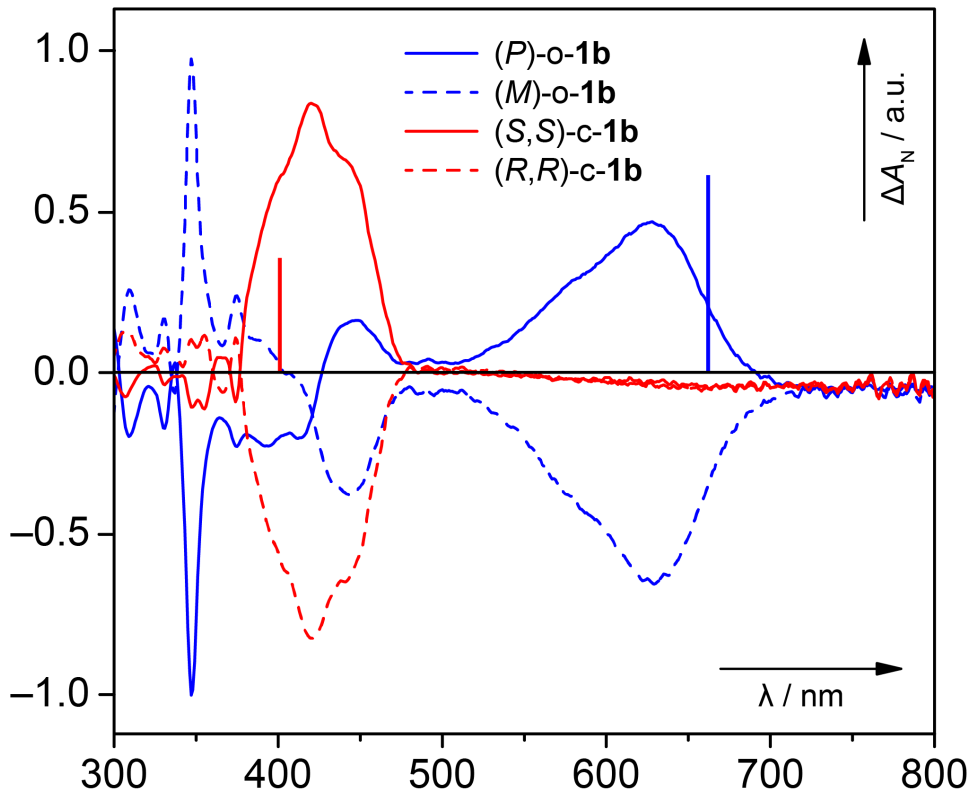


**Figure 4.** CD spectra of the enantiomers of c-**1b** (red traces), separated by HPLC employing a chiral stationary phase, and o-**1b** (blue traces), generated from the enantiomers of c-**1b** upon irradiation (365 nm, 1 min). The spectra were recorded in toluene at 283 K and the absolute configurations were assigned with the aid of TD-DFT calculations (vertical lines; Figure S9).

**DFT Calculations.** The electronic structure of both o-**1b** and c-**1b** in their singlet ground and the lowest triplet excited states as well as the thermally activated conrotatory electrocyclic ring-closure of o-**1b** to c-**1b** were studied with the help of DFT calculations. Among the set of functionals that we employed in our calculations, only the CAM-B3LYP method required the use of broken-symmetry formalism to obtain the structure of o-**1b** in its singlet ground state. Naturally, the optimization of the o-**1b** electrocyclization transition-state structures relied on broken-symmetry wave functions because the ring-closure follows a reaction coordinate of a formally forbidden pericyclic process with an avoided crossing on its symmetric pathway from o-**1b** to c-**1b**. The corresponding activation barriers from the set of used DFT methods are similar, in the range of ~22–24 kcal $mol^{-1}$, and are summarized in Table S3. The calculated singlet–triplet (ST) energy gaps for o-**1b** and c-**1b** are shown in Table S2. The HOMO–LUMO energy gap calculated with the same method (B3LYP/6-311+G(d)) as the one used[11c] previously for parent cethrene (o-**1**) was found to be 1.86 eV (Table S4). The ground-state energy of the closed form c-**1b** is lower by 7.5 kcal $mol^{-1}$ compared to that of the open form o-**1b**.

## DISCUSSION

Diradicaloid π-conjugated molecules have recently regained[1] a considerable interest, although current research has mainly been focused on the physical properties of these systems to understand the relationship between their diradicaloid character and structure. The chemical reactivity that is associated with the diradicaloid character in these polycyclic aromatic hydrocarbons is without doubt of comparable significance, but it remains largely unexplored. Reactions with oxygen, as well as concerted or non-concerted dimer and polymer formations are well known[1a] examples from the early studies of parent systems,[16,17] *ortho*- and *para*-quinodimethanes, or even extended structures[18] such as longer acenes. These reactions

typically represent, however, an undesired feature that impedes the synthesis and isolation of diradicaloid species, and significant efforts have therefore been made[1,19] to develop strategies for decreasing the reactivity, and thus increasing the stability, of these molecules. It has been demonstrated on several occasions that some of the concerted reactions can be reversed, for example, by light irradiation, which offers an opportunity to steer the undesired chemical reactivity of diradicaloids to a useful function. These reactions include thermal dimerization of pleiadene or electrocyclic ring-closure of its dimethyl derivative, both of which can be reversed photochemically, as demonstrated[20] by Michl and co-workers. What links these two examples with cethrene[11a] (o-**1**) and its analog biphenalenylidene[14a] (o-**3**) is low activation energies of their formally symmetry-forbidden thermal electrocyclizations, a feature that arises on account of the diradicaloid character.

In the present study, we took advantage of such unusual reactivity and translated it into a switching function that allows us to turn on and off the two most common characteristics of diradicaloids, namely, small HOMO–LUMO and singlet–triplet (ST) energy gaps. By using 13,14-dimethylcethrene as a model system, we demonstrate that this molecule can act as a diradicaloid switch between an open (o-**1b**) and a closed (c-**1b**) form, where the electrocyclic ring-closure of o-**1b** to thermodynamically more stable c-**1b** can be achieved both thermally and photochemically, while the reversed process, electrocyclic ring-opening of c-**1b** to o-**1b**, can be mediated photochemically. In addition, the helically twisted backbone of cethrene brings an additional element, that of chirality, and this system therefore acts also as a chiroptical switch.

**Synthesis and Properties.** The closed form of 13,14-dimethylcethrene c-**1b** was synthesized (Scheme 2) in eight steps and an overall 17% yield starting from a [5]helicene precursor **5**, which has the two desired methyl substituents already installed in the fjord region, and is equipped with two bromo substituents at positions that allow for a construction of the two

remaining six-membered rings of the cethrene core. The methyl substituents expedite the synthesis of **5**, which can be accessed in only two steps from easily accessible precursors via a series of reactions that we described[15] previously. Moreover, the methyl groups push the configurational stability of the [5]helicene core to the limit set by [9]helicene (the enantiomerization barrier of 10,11-dimethyl[5]helicene is ~44 kcal $mol^{-1}$ at 500 K[15]), making enantio-enriched o-**1b** resistant towards racemization even at elevated temperatures. The solid-state structure of c-**1b** (Figure 2) unambiguously confirms the *anti*-orientation of the methyl groups, which experimentally justifies the conrotatory mode of the electrocyclization of o-**1b** that we could previously support[11a,21] only indirectly.

The open form o-**1b** was generated by irradiation (365 nm, 3 min) of a solution of a pure sample of c-**1b**, during which the NMR resonances that belong to c-**1b** almost completely disappeared and those of o-**1b** became visible. When this solution was left standing at room temperature, all resonances of o-**1b** gradually disappear and those of c-**1b** appear again, as the thermal electrocyclic ring-closure of o-**1b** to c-**1b** takes place.

The open and the closed form have considerably different electronic parameters, namely, the HOMO–LUMO and ST energy gaps. The former is clearly reflected by distinct UV–vis spectra (Figure 3a). While c-**1b** shows absorption mostly in the UV region (red trace), o-**1b** has a characteristic absorption band ($\lambda_{max}$ = 626 nm; $S_0$–$S_1$ transition) in the visible region (blue trace). With regards to the ST gap ($\Delta E_{ST}$), the closed form c-**1b** is computed to have a very high ($\Delta E_{ST}$ ~ 40 kcal $mol^{-1}$, Table S2) and the open form o-**1a** a relatively low ($\Delta E_{ST}$ ~ 10 kcal $mol^{-1}$) triplet energy. EPR spectroscopy was used to probe whether the thermally populated triplet excited state of o-**1b** (Figure 6a) could be detected, as in the case of o-**1a** (ST gap of ~6 kcal $mol^{-1}$, EPR/DFT[11c]). EPR measurements performed on the samples of o-**1b** revealed, however, that this compound is EPR silent at room temperature, which supports that the ST gap of o-**1b** must be larger than that of o-**1a**. The DFT-predicted ST gap

for o-**1b** is even larger than that of EPR-silent planar heptazethrene (~9 kcal mol$^{-1}$, DFT[11c]). The most obvious reason for its increase is a higher degree of helical twist, caused by the steric effect of methyl substituents, which results in a longer distance (3.37 Å) between the fjord carbon atoms compared with that (3.03 Å) of o-**1a** (Figure 5b). The increased distance results in a less efficient through-space orbital overlap within the FMOs (Figure 5a), which is crucial for decreasing the ST gap in o-**1a** relative to heptazethrene.

To assess the geometric effect of the methyl substituents on the ST gap in o-**1b** more quantitatively, we performed relaxed potential energy surface (PES) scans for o-**1** and o-**1b** in their singlet ground and triplet excited states along the coordinate defining the distance (*d*) between the fjord carbon atoms from ~2.8 to 3.9 Å (Figure 5c). In the case of o-**1**, the increase of *d* from 3.03 Å, its minimum-energy value, to 3.37 Å, the minimum-energy value for o-**1b**, resulted in the increase of the ST gap by only 1.2 kcal mol$^{-1}$. In the case of o-**1b**, the ST gap increased comparably by 1.8 kcal mol$^{-1}$. The results of these calculations show that the sole geometric effect of the methyl substituents accounts only for about 30–45% of the ~4 kcal mol$^{-1}$ energy difference between the ST gaps of o-**1** and o-**1b**. The remaining portion can be therefore attributed to the apparently stronger electronic effect of the methyl substituents, which destabilize the LUMO to a higher extent than the HOMO. Dissecting the effect of the methyl groups into electronic and geometric components nicely illustrates the large impact of subtle structural changes on the electronic parameters of helical diradicaloids, which can be employed as a useful tool to fine-tune the properties of this class of materials.

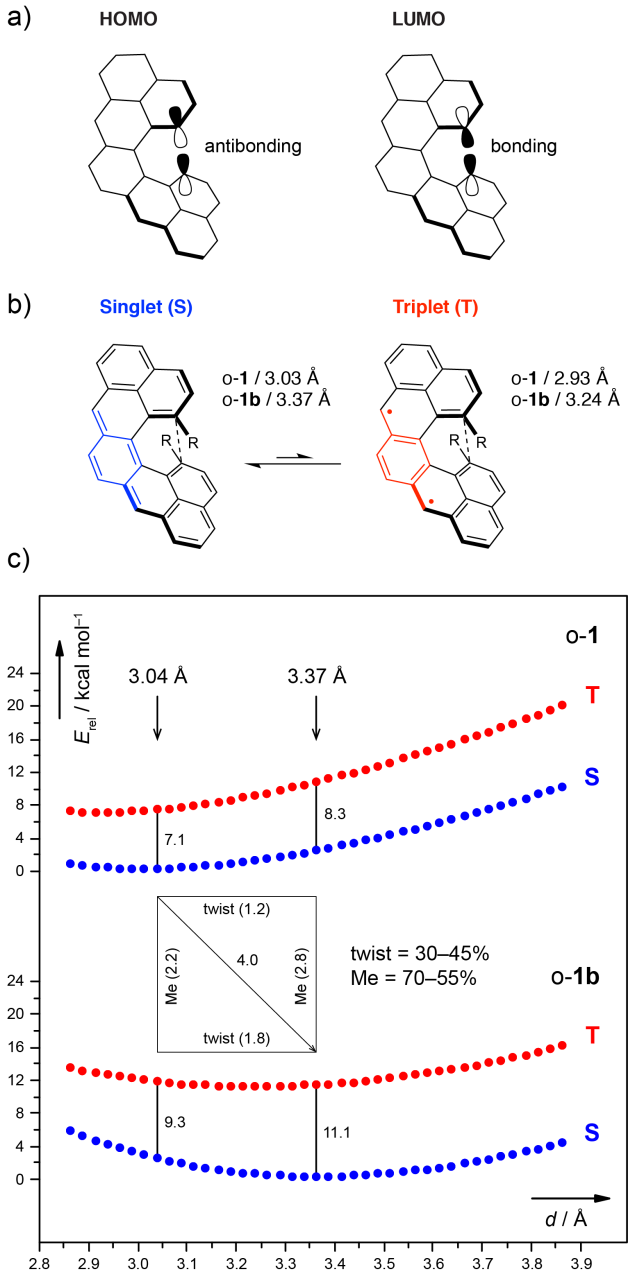


**Figure 5.** (a) Schematic illustration of through-space orbital interactions within the HOMO and the LUMO in o-**1**, o-**1a**, and o-**1b** at positions 13 and 14. (b) Thermal equilibrium between the singlet ground state and the triplet excited state of o-**1** (R = H) and o-**1b** (R = Me). Distances between the fjord carbon atoms (dashed line; distances obtained from optimized geometries (BS/U-B3LYP/6-31G(d)) are shown. (c) Relaxed potential energy surface (PES) scan of o-**1** (top) and o-**1b** (bottom) in their singlet ground (blue) and triplet excited (red) states, which allowed to estimate the relative contributions of the geometric ("twist") and electronic ("Me") effects on the ST gap.

**Switching Parameters.** The kinetics of the thermal ring-closure was studied by UV–vis measurements (Figure 3). It was found that in toluene, the reaction proceeds with an $E_a$ of ~20 kcal mol$^{-1}$, a value that is larger by ~6 kcal mol$^{-1}$ compared to that (~14 kcal mol$^{-1}$) of o-**1a** reported[11a] previously, yet this value is quite small considering the conrotatory ring-closure is formally a forbidden process. The results of our previous studies indicate that the low energies of the first singly and doubly excited states contribute to the lowering of the barrier. The increased $E_a$ in the case of o-**1b** therefore does not come as a surprise, as the HOMO–LUMO gap of o-**1b** (1.86 eV, DFT; 1.80 eV, onset of absorption) is larger than that of o-**1a** (1.68 eV, DFT; 1.70 eV, onset of absorption[11c]), as discussed above.

In a more polar solvent $CH_2Cl_2$, the thermal ring-closure of o-**1b** proceeds faster ($E_a$ ~ 17 kcal mol$^{-1}$) compared to the reaction in toluene. Our DFT calculations show, however, that the electrocyclization barrier for o-**1b** via a $C_2$-symmetric transition state ($E_a$ ~ 22–24 kcal mol$^{-1}$) is insensitive to solvation and compares very well to that calculated previously for o-**1a** ($E_a$ ~ 23 kcal mol$^{-1}$), despite the geometric and electronic changes brought about by the two methyl substituents. These observations are in agreement with our recent hypothesis[11a] that this reaction proceeds not via a $C_2$- but a $C_1$-symmetric transition state that has a partial charge-transfer character. In addition, an alternate mechanism that could involve a radical-cation intermediate can now be also safely dismissed, as no oxidant was present in the sample of o-**1b** generated from a pure sample of c-**1b** solely by light.

The chirality and the distinct electronic properties (HOMO–LUMO and ST energy gaps) of o-**1b** and c-**1b** attracted our attention to investigate 13,14-dimethylcethrene as a conceptually new model for the design of chiroptical magnetic switches that could be operated solely by light. The photochemical processes, namely, ring-opening of c-**1b** and the reversed process, ring-closure of o-**1b**, were therefore studied by means of NMR (Figure 1), UV–vis (Figure 3), and CD (Figure 4) spectroscopies. In accord with the Woodward–Hoffmann rules,[13] both

conrotatory reactions proceed readily, with irradiation times of 1 min being sufficient for achieving a full conversion at concentrations of ~$10^{-4}$ M. This allows for efficient switching from the closed to the open form by UV light (365 nm), and from the open to the closed form by visible light (630 nm). The full irradiation cycle is shown in Figure 6a, where a colorless solution of c-**1b** is irradiated at 365 nm affording a blue solution of o-**1b**, which upon irradiation at 630 nm turns into a colorless solution of c-**1b** (see also the video supporting material). The robustness of this system was demonstrated by repeating the full irradiation cycle multiple times in an aerated solution (Figure 6b). Under these conditions, the system showed only a moderate decomposition (~1.5% loss of absorbance per cycle). The same degree of decomposition was observed when the irradiation cycles were performed under an inert atmosphere (Figures S5–S7), which indicates that the decomposition pathway of photoexcited o-**1b** or c-**1b** does not involve reactions with oxygen.

Although o-**1b** possesses an ST gap that is too large for a detection of an EPR signal required for having a true magnetic switch, the electronic effect of the methyl substituents on the ST gap, demonstrated clearly by our DFT calculations, holds promise for achieving such task. Installment of additional suitable substituents at relevant positions of the cethrene core, where the orbital coefficients in the HOMO and the LUMO differ markedly, should result in a decrease of the ST gap in a derivative of o-**1b**. Work on such system is in progress in our laboratories.

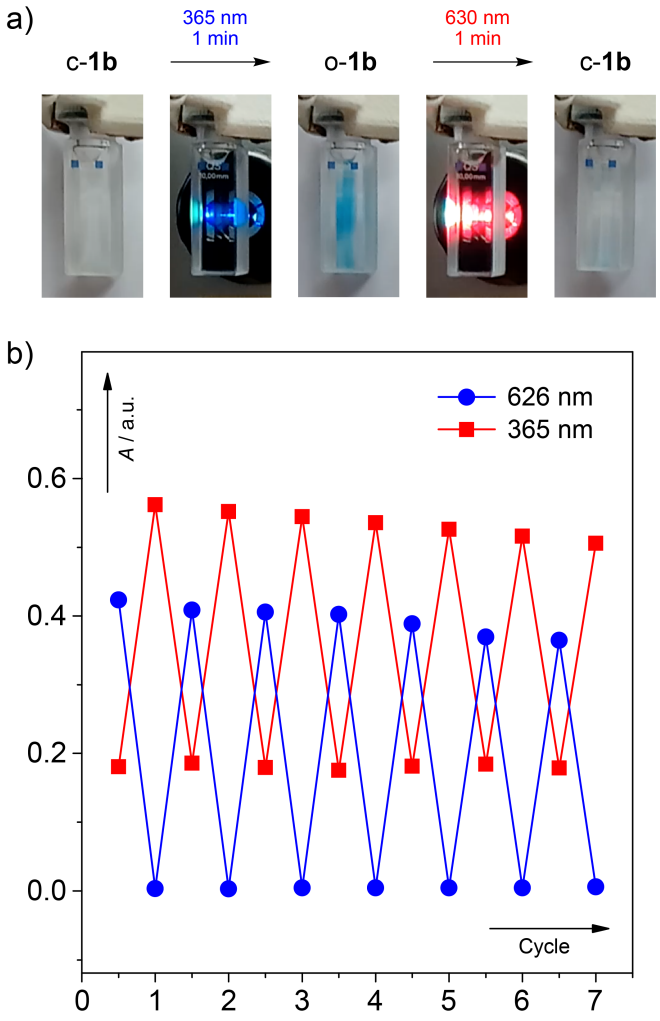


**Figure 6.** (a) Photographs documenting one full irradiation cycle. (b) A graph showing the drops and jumps of absorbance at 365 and 626 nm of a solution of c-**1b** in toluene (~$10^{-4}$ M, 298 K) under aerated conditions over seven irradiation cycles.

## CONCLUSION

We demonstrated that installment of two methyl substituents in the fjord region of cethrene leads to a robust system, where chemical reactivity of the diradicaloid core can be turned into a switching function. The methyl substituents do not only improve stability of this system against oxidation but also racemization, and expedite the synthesis. Kinetic studies of the thermal electrocyclic ring-closure of the open form bring further evidence that supports our

hypothesis that the thermal electrocyclization proceeds via a $C_1$-symmetric transition state. Photochemical studies reveal that, in accord with the Woodward–Hoffmann rules, the conrotatory electrocyclic ring-closure and ring-opening can be efficiently mediated by visible and UV light, respectively. On account of the distinct electronic and geometric parameters of the open and the closed form, namely, the HOMO–LUMO and ST energy gaps and the degree of helical twist, the switching process can be monitored by a variety of spectroscopic techniques, which illustrate that this system functions as a chiroptical diradicaloid photoswitch. Moreover, substantial alteration of the ST gap upon switching suggests that the 13,14-dimethylcethrene structural motif, or related structures, can be employed in a conceptually new design of all-organic chiral magnetic switches that can be operated solely by light.

## EXPERIMENTAL SECTION

**Synthesis and Characterization.** Experimental procedures and characterization data for all new compounds described in this work are compiled in the Supporting Information (Sections S1, S6, S7, and S8). Compound **5** was described[15] previously and was prepared according to the published protocols. All chemicals and solvents were purchased from commercial sources and were used without further purification unless stated otherwise. The reactions and experiments that are sensitive to oxygen were performed using Schlenk techniques and argon-saturated solvents. The solvents were saturated with argon by either passing argon gas through the solvent or using the freeze-pump-thaw technique in three cycles. The NMR experiments were performed on instruments operating at 400, 500, or 600 MHz proton frequencies. The instruments were equipped with a direct-observe 5 mm BBFO smart probe (400 and 600 MHz), an indirect-detection 5 mm BBI probe (500 MHz), or a five-channel cryogenic 5 mm QCI probe (600 MHz). All probes were equipped with actively shielded *z*-

gradients (10 A). The experiments were performed at 295 or 298 K unless indicated otherwise and the temperatures were calibrated using a methanol standard showing accuracy within ±0.2 K. Standard pulse sequences were used and the data was processed using two-fold zero-filling in the indirect dimension for all 2D experiments. The highly deuterium-enriched benzene ($C_6D_6$, >99.96% D) was used in NMR experiments. Chemical shifts ($\delta$) are reported[22] in parts per million (ppm) relative to the solvent residual peak ($^1$H and $^{13}$C NMR, respectively): $C_6D_6$ ($\delta$ = 7.16 and 128.06 ppm), $CD_2Cl_2$ ($\delta$ = 5.32 and 53.84 ppm), and $CD_3SOCD_3$ ($\delta$ = 2.50 and 39.52 ppm). The UV–Vis spectra were recorded in toluene or $CH_2Cl_2$ at room temperature. The HPLC separation of enantiomers of c-**1b** was performed on an HPLC instrument equipped with a diode array UV–vis detector ($\lambda$ = 200–600 nm) and a chiral-stationary-phase column (Chiralpak IA, 0.46 × 25 cm). Sample injection: 25 µL of a solution of c-**1b** in *n*-heptane/*t*-BuMeO (1:1, ~1 mg in 1 mL). Separation: *n*-heptane/*t*-BuMeO (98:2), flow rate 1.0 mL min$^{-1}$, 293 K. The CD spectra were recorded in toluene at 283 K in a 1 cm quartz glass cuvette. All solutions were prepared and measured under argon-saturated conditions unless stated otherwise.

**Single-Crystal X-Ray Diffraction (XRD).** Single crystals of compound **7** suitable for X-ray diffraction analysis were grown from the corresponding solution in $CH_2Cl_2$ by slow evaporation of the solvent. Data collections for this structure was performed at low temperatures (123 K) using CuKα radiation on a Bruker APEX II diffractometer. Integration of the frames and data reduction was carried out using[23] the *APEX2* software. The structure was solved by the charge-flipping method using[24] *Superflip*. All non-hydrogen atoms were refined anisotropically by full-matrix least-squares on $F^2$ using[25] *CRYSTALS*. Single crystals of compound c-**1b** suitable for X-ray diffraction analysis were grown from the corresponding solution in hexane by slow evaporation of the solvent in the dark. Diffraction data were collected at 160(1) K on a Rigaku OD XtaLAB Synergy, Dualflex, Pilatus 200K

diffractometer using a single-wavelength X-ray source (MoKα radiation: λ = 0.71073 Å)[26] from a micro-focus sealed X-ray tube and an Oxford liquid-nitrogen Cryostream cooler. The selected suitable single crystal was mounted using polybutene oil on a flexible loop fixed on a goniometer head and immediately transferred to the diffractometer. Pre-experiment, data collection, data reduction, and analytical absorption correction[27] were performed[28] with the program suite *CrysAlisPro*. Using *Olex2*,[29] the structure was solved with the SHELXT[30] small-molecule structure-solution program and refined with the *SHELXL2016/6* program package[31] by full-matrix least-squares minimization on $F^2$. *PLATON*[32] was used to check the result of the X-ray analysis. For more details about the data collection and refinement parameters of both compounds, see the corresponding CIF files. Both structures were analyzed using[33] Mercury. The crystallographic views of their solid-state structures are shown in Figures S10 (**7**) and S11 (c-**1b**). The crystal parameters and structure refinements are summarized below and in Table S1. The crystallographic parameters were deposited into the Cambridge Crystallographic Data Centre (CCDC).

**Crystal Parameters for Compound 7.** $C_{30}H_{22}O_2$; 0.04 × 0.08 × 0.08 mm; monoclinic, *C*2/*c* (No. 15); $a$ = 9.2601(11), $b$ = 14.9860(11), and $c$ = 14.9657(14) Å; $\alpha$ = 90, $\beta$ = 107.491(4), and $\gamma$ = 90°; $V$ = 1980.8(3) Å$^3$; $Z$ = 4; $T$ = 123 K; $\rho_{calc}$ = 1.390 g cm$^{-3}$; $\mu$ = 0.670 mm$^{-1}$. CCDC no.: 1563973.

**Crystal Parameters for Compound c-1b.** $C_{30}H_{20}$; 0.09 × 0.14 × 0.21 mm; monoclinic, *P*2$_1$/*c* (No. 14); $a$ = 7.82299(16), $b$ = 17.3405(4), and $c$ = 13.9697(3) Å; $\alpha$ = 90, $\beta$ = 96.824(2), and $\gamma$ = 90°; $V$ = 1881.62(7) Å$^3$; $Z$ = 4; $T$ = 160(1) K; $\rho_{calc}$ = 1.343 g cm$^{-3}$; $\mu$ = 0.076 mm$^{-1}$. CCDC no.: 1563974.

**UV–Vis Kinetic Measurements.** The activation energy ($E_a$) for the thermal transformation of o-**1b** to c-**1b** was determined through kinetic measurements. A solution of c-**1b** in $CH_2Cl_2$ or toluene (~$10^{-4}$ M) was irradiated at 365 nm for 2.5 min at room temperature, whereupon a

majority of c-**1b** was converted to o-**1b**. The UV–vis spectra before and after irradiation are shown in Figures S1a ($CH_2Cl_2$) and S2a (toluene). The absorption band with a maximum at 624 nm ($CH_2Cl_2$) and 626 nm (toluene) corresponds to o-**1b** ($S_0$–$S_1$ transition). As this band does not have any overlap with absorption bands of c-**1b**, the decrease of this band's maximum intensity (Figures S1b and S2b) was used for determination of the rate constants ($k$) at various temperatures (Figures S3a and S4a). Because the electrocyclization of o-**1b** to give c-**1b** is a unimolecular process, it was assumed that this transformation follows the first-order kinetics ($\ln(A_t/A_0) = -kt$). The $\ln(k)$ values were plotted against $1/T$ (Figures S3b and S4b) and the Arrhenius equation ($\ln(k) = \ln(A) - E_a/(RT)$) was then used to determine the values of $E_a$ in $CH_2Cl_2$ and toluene.

**DFT Calculations.** The DFT calculations were performed in Gaussian 09[34] (Revision D.01) suite of electronic structure programs. The gas-phase geometry optimizations were done with the respective functional (B3LYP, CAM-B3LYP, BMK, or M06-2X) and the 6-31G(d) or 6-311+G(d) basis sets, and ultrafine integration grid (Integral=Ultrafine keyword in Gaussian). Frequency analysis was performed to test the character of the stationary points and to provide zero-point vibrational energy corrections (ZPVEs), which were used unscaled. The geometries obtained with the latter basis set were used for calculations of the optical properties. The restricted ("R-" prefix) formalism was used to model the singlet states and the unrestricted ("U-" prefix) formalism was used in the modeling of the triplet states. The solution of the SCF equations for the restricted singlet wavefunctions was tested for stability and optimized to obtain the lowest energy if an RHF→UHF instability was found (Stable=Opt keyword in Gaussian). The broken-symmetry (BS) singlet wavefunction obtained this way was used to reoptimize the geometries of the molecules. The final energies were calculated with the cc-pVTZ basis set either employing the polarizable continuum model (PCM; with PhMe as the solvent) to account for the collective solvation effects in

calculations of light absorption properties or in the gas phase otherwise. The relaxed potential energy surface scans (Figure 6) along the coordinate that describes the distance between the carbon 13 and 14 in o-**1** and o-**1b** were performed for both the singlet ground and the lowest triplet states for both the singlet ground and the lowest triplet states at the B3LYP/6-31G(d) level of theory with no solvation and ZPVE corrections. The TD-DFT/cc-pVDZ calculations served to predict the absorption properties of o-**1b**, and to model the circular dichroism (CD) spectra of the enantiomers of o-**1b** and c-**1b** (see Figure 4).

## ASSOCIATED CONTENT

### Supporting Information

The Supporting Information is available free of charge on the ACS Publications website.

Synthetic procedures and characterization data for all new compounds, UV–vis, HPLC, CD, and crystallographic data, results of DFT calculations, assignment of $^{1}H$ and $^{13}C$ NMR resonances, copies of NMR and HRMS spectra, and Cartesian coordinates for all optimized geometries (PDF)

Crystallographic data (CIFs) for **7** and c-**1b**

Video-documentation of the photochemical switching (MP4)

## AUTHOR INFORMATION

### Corresponding Author

michal.juricek@chem.uzh.ch

### Notes

The authors declare no competing financial interest.

## ACKNOWLEDGEMENTS

This project has received funding from the European Research Council (ERC) under the European Union's Horizon 2020 research and innovation programme (Grant Agreement No. 716139), the Swiss National Science Foundation (SNSF, M.J./PZ00P2_148043 and PP00P2_170534), the Novartis University of Basel Excellence Scholarship (P.R. and M.J.), and the Experientia Foundation (T.Š.). We thank Prof. Dr. Marcel Mayor for a generous support of our research at the University of Basel (UB) and Dr. Alessandro Prescimone (UB) for X-ray crystallographic analysis of **7**, and gratefully acknowledge the computational facilities of the University of Fribourg.

## REFERENCES

(1) (a) Konishi, A.; Kubo, T. *Top. Curr. Chem.* **2017**, *375*, 83. (b) Konishi, A.; Kubo, T. In *Chemical Science of π-Electron Systems*; Akasaka, T.; Osuka, A.; Fukuzumi, S.; Kandori, H.; Aso, Y., Eds.; Springer: Tokyo, Japan, **2015**; pp 337–360. (c) Kubo, T. *Chem. Rec.* **2015**, *15*, 218–232. (d) Sun, Z.; Zeng, Z.; Wu, J. *Acc. Chem. Res.* **2014**, *47*, 2582–2591. (e) Abe, M. *Chem. Rev.* **2013**, *113*, 7011–7088. (f) Morita, Y.; Suzuki, S.; Sato, K.; Takui, T. *Nat. Chem.* **2011**, *3*, 197–204. (g) Morita, Y.; Nishida, S. In *Stable Radicals: Fundamentals and Applied Aspects of Odd-Electron Compounds*; Hicks, R. G., Ed.; John Wiley & Sons, Ltd.: Wiltshire, U.K., **2010**; pp 81–145.

(2) (a) Pal, S. K.; Itkis, M. E.; Tham, F. S.; Reed, R. W.; Oakley, R. T.; Haddon, R. C. *Science* **2005**, *309*, 281–284. (b) Kubo, T.; Shimizu, A.; Sakamoto, M.; Uruichi, M.; Yakushi, K.; Nakano, M.; Shiomi, D.; Sato, K.; Takui, T.; Morita, Y.; Nakasuji, K. *Angew. Chem. Int. Ed.* **2005**, *44*, 6564–6568. (c) Itkis, M. E.; Chi, X.; Cordes, A. W.; Haddon, R. C. *Science* **2002**, *296*, 1443–1445.

(3) (a) Michl, J.; Bonačić-Koutecký, V. *Tetrahedron* **1988**, *44*, 7559–7585. (b) Salem, L.; Rowland, C. *Angew. Chem. Int. Ed.* **1972**, *11*, 92–111.

(4) (a) Kubo, T.; Katada, Y.; Shimizu, A.; Hirao, Y.; Sato, K.; Takui, T.; Uruichi, M.; Yakushi, K.; Haddon, R. C. *J. Am. Chem. Soc.* **2011**, *133*, 14240–14243. (b) Goto, K.; Kubo, T.; Yamamoto, K.; Nakasuji, K.; Sato, K.; Shiomi, D.; Takui, T.; Kubota, M.; Kobayashi, T.; Yakusi, K.; Ouyang, J. *J. Am. Chem. Soc.* **1999**, *121*, 1619–1620.

(5) (a) Cui, Z.-H.; Lischka, H.; Beneberu, H. Z.; Kertesz, M. *J. Am. Chem. Soc.* **2014**, *136*, 5539–5542. (b) Mou, Z.; Uchida, K.; Kubo, T.; Kertesz, M. *J. Am. Chem. Soc.* **2014**, *136*, 18009–18022. (c) Cui, Z.-H.; Lischka, H.; Beneberu, H. Z.; Kertesz, M. *J. Am. Chem. Soc.* **2014**, *136*, 12958−12965. (d) Tian, Y.-H.; Huang, J.; Kertesz, M. *Phys. Chem. Chem. Phys.* **2010**, *12*, 5084–5093. (e) Miller, J. S.; Novoa, J. J. *Acc. Chem. Res.* **2007**, *40*, 189–196. (f) Suzuki, S.; Morita, Y.; Fukui, K.; Sato, K.; Shiomi, D.; Takui, T.; Nakasuji, K. *J. Am. Chem. Soc.* **2006**, *128*, 2530–2531. (g) Takano, Y.; Taniguchi, T.; Isobe, H.; Kubo, T.; Morita, Y.; Yamamoto, K.; Nakasuji, K.; Takui, T.; Yamaguchi, K. *J. Am. Chem. Soc.* **2002**, *124*, 11122–11130.

(6) Mou, Z.; Kertesz, M. *Angew. Chem. Int. Ed.* **2017**, *56*, 10188–10191.

(7) Das, A.; Müller, T.; Plasser, F.; Lischka, H. *J. Phys. Chem. A* **2016**, *120*, 1625–1636.

(8) Takamuku, S.; Nakano, M.; Kertesz, M. *Chem. Eur. J.* **2017**, *23*, 7474–7482.

(9) Rickhaus, M.; Mayor, M.; Juríček, M. *Chem. Soc. Rev.* **2016**, *45*, 1542–1556.

(10) Juríček, M. *Chimia* **2018**, *72*, DOI: 10.2533/chimia.2018.1.

(11) (a) Šolomek, T.; Ravat, P.; Mou, Z.; Kertesz, M.; Juríček, M. *J. Org. Chem.* **2018**, *83*, 4769–4774. (b) Ravat, P.; Šolomek, T.; Ribar, P.; Juríček, M. *Synlett* **2016**, *27*, 1613–1617. (c) Ravat, P.; Šolomek, T.; Rickhaus, M.; Häussinger, D.; Neuburger, M.; Baumgarten, M.; Juríček, M. *Angew. Chem. Int. Ed.* **2016**, *55*, 1183–1186.

(12) (a) Li, Y.; Heng, W.-K.; Lee, B. S.; Aratani, N.; Zafra, J. L.; Bao, N.; Lee, R.; Sung, Y. M.; Sun, Z.; Huang, K.-W.; Webster, R. D.; López Navarrete, J. T.; Kim, D.; Osuka, A.; Casado, J.; Ding, J.; Wu, J. *J. Am. Chem. Soc.* **2012**, *134*, 14913–14922. (b) Clar, E.; Macpherson, I. A. *Tetrahedron* **1962**, *18*, 1411–1416.

(13) (a) Woodward, R. B.; Hoffmann, R. *The Conservation of Orbital Symmetry*; Verlag Chemie: Weinheim, **1970**. (b) Fleming, I. *Molecular Orbitals and Organic Chemical Reactions*; Wiley: Chichester, **2010**; pp. 253–368. (c) Woodward, R. B.; Hoffmann, R. *Angew. Chem. Int. Ed.* **1969**, *8*, 781–932. (d) Woodward, R.; Hoffmann, R. *J. Am. Chem. Soc.* **1965**, *87*, 295–397.

(14) (a) Uchida, K.; Ito, S.; Nakano, M.; Abe, M.; Kubo, T. *J. Am. Chem. Soc.* **2016**, *138*, 2399–2410. (b) Pogodin, S.; Agranat, I. *J. Am. Chem. Soc.* **2003**, *125*, 12829–12835.

(15) Ravat, P.; Hinkelmann, R.; Steinebrunner, D.; Prescimone, A.; Bodoky, I.; Juríček, M. *Org. Lett.* **2017**, *19*, 3707–3710.

(16) (a) Segura, J. L.; Martín, N. *Chem. Rev.* **1999**, *99*, 3199–3246. (b) Charlton, J. L.; Alauddin, M. M. *Tetrahedron* **1987**, *43*, 2873–2889.

(17) Brown, C. J.; Farthing, A. C. *Nature* **1949**, *164*, 915–916.

(18) Zade, S. S.; Bendikov, M. *J. Phys. Org. Chem.* **2012**, *25*, 452–461.

(19) Anthony, J. E. *Chem. Rev.* **2006**, *106*, 5028–5048.

(20) (a) Steiner, R. P.; Michl, J. *J. Am. Chem. Soc.* **1978**, *100*, 6413–6415. (b) Kolc, J.; Michl, J. *J. Am. Chem. Soc.* **1970**, *92*, 4147–4148.

(21) Although there was some structural ambiguity around the $sp^3$-carbon atoms in the solid-state structure of c-**3** obtained from crystallographic analysis on account of disordered alignment of the (*R*,*R*) and (*S*,*S*) enantiomers, the planar molecular backbone indicated the *anti*-configuration of c-**3** (see ref. 14a).

(22) Fulmer, G. R.; Miller, A. J. M.; Sherden, N. H.; Gottlieb, H. E.; Nudelman, A.; Stoltz, B. M.; Bercaw, J. E.; Goldberg, K. I. *Organometallics* **2010**, *29*, 2176–2179.

(23) *Bruker Analytical X-ray Systems, Inc., APEX2, Version 2 User Manual, M86–E01078*; Bruker: Madison WI, **2006**.

(24) Palatinus, L.; Chapuis, G. *J. Appl. Crystallogr.* **2007**, *40*, 786–790.

(25) Betteridge, P. W.; Carruthers, J. R.; Cooper, R. I.; Prout, K.; Watkin, D. J. *J. Appl. Crystallogr.* **2003**, *36*, 1487.

(26) Rigaku Oxford Diffraction, **2015**.

(27) Clark, R. C.; Reid, J. S. *Acta Crystallogr. A* **1995**, 51, 887–897.

(28) *CrysAlisPro (version 1.171.39.13a)*; Rigaku Oxford Diffraction, **2016**.

(29) Dolomanov, O. V.; Bourhis, L. J.; Gildea, R. J.; Howard, J. A. K.; Puschmann, H. *J. Appl. Crystallogr.* **2009**, *42*, 339–341.

(30) Sheldrick, G. M. *Acta Crystallogr. A* **2015**, *71*, 3–8.

(31) Sheldrick, G. M. *Acta Crystallogr. C* **2015**, *71*, 3–8.

(32) Spek, A. L. *J. Appl. Crystallogr.* **2003**, *36*, 7–13.

(33) (a) Macrae, C. F.; Bruno, I. J.; Chisholm, J. A.; Edgington, P. R.; McCabe, P.; Pidcock, E.; Rodriguez-Monge, L.; Taylor, R.; van de Streek, J.; Wood, P. A. *J. Appl. Crystallogr.* **2008**, *41*, 466–470. (b) Bruno, I. J.; Cole, J. C.; Edgington, P. R.; Kessler, M.; Macrae, C. F.; McCabe, P.; Pearson, J.; Taylor, R. *Acta Crystallogr. B* **2002**, *58*, 389–397.

(34) Frisch, M. J.; Trucks, G. W.; Schlegel, H. B.; Scuseria, G. E.; Robb, M. A.; Cheeseman, J. R.; Scalmani, G.; Barone, V.; Petersson, G. A.; Nakatsuji, H.; Li, X.; Caricato, M.; Marenich, A. V.; Bloino, J.; Janesko, B. G.; Gomperts, R.; Mennucci, B.; Hratchian, H. P.; Ortiz, J. V.; Izmaylov, A. F.; Sonnenberg, J. L.; Williams-Young, D.; Ding, F.; Lipparini, F.; Egidi, F.; Goings, J.; Peng, B.; Petrone, A.; Henderson, T.; Ranasinghe,

D.; Zakrzewski, V. G.; Gao, J.; Rega, N.; Zheng, G.; Liang, W.; Hada, M.; Ehara, M.; Toyota, K.; Fukuda, R.; Hasegawa, J.; Ishida, M.; Nakajima, T.; Honda, Y.; Kitao, O.; Nakai, H.; Vreven, T.; Throssell, K.; Montgomery, J. A., Jr.; Peralta, J. E.; Ogliaro, F.; Bearpark, M. J.; Heyd, J. J.; Brothers, E. N.; Kudin, K. N.; Staroverov, V. N.; Keith, T. A.; Kobayashi, R.; Normand, J.; Raghavachari, K.; Rendell, A. P.; Burant, J. C.; Iyengar, S. S.; Tomasi, J.; Cossi, M.; Millam, J. M.; Klene, M.; Adamo, C.; Cammi, R.; Ochterski, J. W.; Martin, R. L.; Morokuma, K.; Farkas, O.; Foresman, J. B.; Fox, D. J. Gaussian 09, Revision D.01, Gaussian, Inc., Wallingford CT, **2009**.